A quality control procedure for Fengyun-3A microwave temperature sounder with emphasis on a new cloud detection algorithm

Xiang Wang,[1] Yifang Ren[2] and Gang Li[3]

[1] Centre of Data Assimilation for Research and Application, Nanjing University of Information Science & Technology, Nanjing, China
[2] Jiangsu Meteorological Service, Jiangsu Meteorological Administration, Nanjing, China
[3] Centre of Data Assimilation for Research and Application, Nanjing University of Information Science & Technology, Nanjing, China

(Manuscript received June 2015; accepted March 2016)

A cloud detection algorithm for satellite radiance from the microwave temperature sounder (MWTS) on board the first satellite of the Chinese polar-orbiting Fengyun-three series (FY-3A) is proposed based on the measurements at the frequencies of 50.3 and 53.6 GHz. The cloud liquid water path index (LWP index) is calculated using the brightness temperature at these two channels. Analysis of one case carried out in January 2010 shows the great consistency between this new algorithm result and the available liquid water path product from the Meteorological Operational satellite A (MetOp-A). In general, about 60% of the global MWTS data are considered to be contaminated by cloud by virtue of the new cloud detection algorithm. A quality control (QC) procedure is applied to MWTS measurements with emphasis on the cloud detection. The QC steps are composed of (i) channel 2 over sea ice, land and coastal field of views (FOVs); (ii) channels 2 and 3 over cloudy FOVs; and (iii) outliers with large differences between observations and model simulations. After QC, MWTS measurements of channels 2–4 agree very well with the model simulations using the National Centres for Environmental Prediction (NCEP) forecast data as radiative transfer model input; the scan biases are reduced significantly, especially at the edges of the swath; and the frequency distributions of the differences between observations and model simulations become more Gaussian-like.

1. Introduction

On 27 May 2008, the first satellite in the new Chinese polar-orbiting satellites Fengyun series (FY-3A) was successfully launched into a circular, sun-synchronous, near-polar and morning-configured (10.00 am, mean equator crossing local solar time of the descending node) orbit with an altitude of 836 km above the Earth and an inclination angle of 98.75°. Eleven instruments are on board FY-3A, including: Visible and InfRared Radiometer (VIRR); MEdium ReSolution Imager (MERSI); InfRared Atmospheric Sounder (IRAS); MicroWave Temperature Sounder (MWTS); MicroWave Humidity Sounder (MWHS); MicroWave Radiation Imager (MWRI); Solar Backscatter Ultraviolet Sounder (SBUS); Total Ozone Mapping Unit (TOU); Earth Radiation Measurer (ERM); Solar Irradiation Monitor (SIM); and Space Environment Monitor (SEM) (Dong et al. 2009). The performance of the atmospheric sounding instruments meets or exceeds the prelaunch

Corresponding author: Xiang Wang, 219# Ningliu Road, Pukou district, Nanjing, Jiangsu, China,
Email: wangxiang@nuist.edu.cn

specifications (Yang et al. 2009). MWTS is a four-channel cross-track radiometer that is similar to Advanced Microwave Sounding Unit-A (AMSU-A) channels 3, 5, 7 and 9 on board NOAA-15 to 19 (You et al. 2012). Adjoint-based estimates of observation impacts on numerical weather prediction (NWP) (Baker and Daley 2000) have demonstrated that the largest error decreases per instrument type is due to AMSU-A (Cardinali 2009, Fourrie et al. 2002, Langland and Baker 2004). It is undoubtedly recognised that direct assimilation of AMSU-A sounding channels measurements can significantly improve the accuracy of weather analysis and forecasts (Andersson et al. 1994, Courtier et al. 1998, Derber and Wu 1998, McNally et al. 2000, Zhang et al. 2004, Kozo et al. 2005). Similarly, it is of great value to incorporate the MWTS data from the FY-3 series into NWP models (Li and Zou 2014).

Quality control (QC) is important for assimilation of any satellite data. Observations have errors, forward models have limitations and forecast models have uncertainty. Since data assimilation systems are very sensitive to erroneous observations and are inclined to converge towards outliers, observations that are either unreliable or cannot be simulated accurately must be identified and eliminated before being assimilated. Development of an effective QC procedure is thus important for all observations to optimally improve numerical weather forecasts. MWTS is the first atmospheric sounding instrument developed by China, and it is important to have an effective and efficient QC procedure for MWTS measurements from the FY-3 series before being incorporated into the Chinese NWP or other data assimilations systems.

The analysis can be greatly improved based on the successful satellite data assimilation, which can benefit the numeric weather prediction, so the MWTS data might be useful for NWP modelling systems if properly assimilated. Challenges to the assimilation of satellite radiance measurements are associated with radiance biases, cloud contamination and surface emissivity. Microwave radiation at MWTS frequencies can penetrate through clouds except for the heavy precipitation. MWTS radiance measurements in non-heavy precipitation contain useful information about clouds and precipitation. However, it is difficult to simulate the cloud-contaminated radiances accurately using a radiative transfer model. So far, the cloud-affected microwave imager radiances assimilation have only been done operationally by ECMWF (Bauer et al. 2006, Bauer et al. 2010). As a first step towards the assimilation of all-weather data, our current work is to assimilate clear-sky microwave temperature sounding observations. Therefore, data in cloudy conditions should be eliminated based on effective cloud detection algorithms.

There were couples of cloud detection algorithms developed for satellite microwave measurements. The cloud detection method for special sensor microwave imager (SSM/I) radiance is based on the cloud liquid water path (LWP) retrieved using water vapour and cloud liquid water sensitive channels (Weng and Grody 1994). Soon after, this method was applied to AMSU-A based on channels 1 and 2 (Weng et al. 2003). The scatter index (SI) method is implemented to the Advanced Tiros Operational Vertical Sounder (ATOVS) and Advanced Very High Resolution Radiometer (AVHRR) data to detect scattering hydrometeors over ocean (Klaes and Schraidt 1999), where SI is defined by the difference between AMSU-A channel 15 observations and simulations using a linear regression model. However, these algorithms are mainly developed for the microwave instruments with the two water vapour and cloud liquid water sensitive channels which are not available for FY-3A MWTS. Therefore, a cloud detection algorithm is incorporated based on the cloud fraction product provided by the Visible and InfrarRed Radiometer (VIRR) on board FY-3A (Li and Zou 2013), which is one of the advantages of having the VIRR on board the same satellite platform as the MWTS.

This paper is organised as follows: Section 2 will briefly present the major instrument characteristics of FY-3A MWTS. Model simulations of MWTS are provided in this section too. A cloud detection methodology based on MWTS measurements themselves will be described and the effectiveness then will be validated in Section 3. Section 4 presents the quality control procedure with emphasis on the cloud detection, and shows some numerical results before and after QC. The conclusions are drawn in Section 5.

2. MWTS instrument characteristics and model simulations

2.1 MWTS instrument characteristics

MWTS is a total power radiometer and scans in a cross track manner within ±48.3° with respect to the nadir direction. MWTS only has four channels in the oxygen band at frequencies ranging from 50.3 to 57.3 GHz for temperature sounding from the surface to about 1 hPa because of the absorption and emission of microwave radiation by atmospheric oxygen. MWTS provides only a total of 15 field of views (FOVs) along each scan line. The observation resolution at nadir for MWTS is about 62 km. Table 1 lists a few selected channel characteristics of MWTS, includ-

ing channel frequency, peak weighting function height, measurement precision, noise-equivalent delta temperature (NEDT), and 3 dB band width (Dong et al. 2009). The two-point calibration technique for AMSU-A (Mo 1999) is used for the calibration of the MWTS data (You et al. 2012). The MWTS channel 1 frequency is centred at 50.3 GHz and is sensitive to surface and cloud liquid water, while channels 2-4 are for the sounding of the atmospheric temperature in the troposphere and low stratosphere.

Channel	*Frequency (GHz)*	*WF (hPa)*	*NEDT (K)*	*Nadir FOV (km)*	*Bandwidth (MHz)*
1	50.30	Surface	0.5	62	180
2	53.59	700	0.4	62	340
3	54.94	300	0.4	62	400
4	57.29	90	0.4	62	330

Table 1 Channel characteristics of FY-3A MWTS

2.2 Model simulations

In this study, the community radiative transfer model (CRTM) developed by the US Joint Centre for Satellite Data Assimilation (JCSDA) for rapid calculations of satellite radiances is used to produce global simulations of brightness temperatures that are measured by MWTS (Weng 2007, Han et al. 2007). The vertical profiles of pressure, temperature, and specific humidity, the surface parameters of surface skin temperature, 2-m wind speed, and wind direction from the NCEP Global Forecast System (GFS) 6-h forecasts are used as input to CRTM, along with sensor's zenith angle serving as additional input to CRTM. The NCEP GFS 6-h forecast fields have a horizontal resolution 0.3125° × 0.3125° and 64 vertical levels, with the highest vertical level located near 0.1 hPa.

Global simulations of brightness temperature can be usually used as a 'reference' or 'truth' for examining the performance of the MWTS instrument. Statistical features of the differences between the MWTS observed and model-simulated brightness temperatures are examined.

3. Cloud detection methodology and validation

3.1 Methodology

As demonstrated by Weng et al. (2003), microwave measurements at lower frequency window channels can be directly related to LWP through an emission-based radiative transfer model, in which the effects of surface parameters such as emissivity and temperature on the measurements at two channels are taken into account. Specifically, cloud LWP over ocean can be derived by the following formula:

$$L = a_0\mu[ln(T_s - T_b^{31}) - a_1 ln(T_s - T_b^{23}) - a_2] \quad (1)$$

Where coefficients a_0, a_1 and a_2 are calculated by

$$a_0 = -0.5\,\omega_v^{23}/(\omega_v^{23}\omega_l^{31} - \omega_v^{31}\omega_l^{23}) \quad (2)$$

$$a_1 = \omega_v^{31}/\omega_v^{23} \quad (3)$$

$$a_2 = -2.0\,(\tau_0^{31} - a_1\tau_0^{23})/\mu + (1.0 - a_1)ln(T_s) + ln(1.0 - \varepsilon^{31}) - a_1 ln(1.0 - \varepsilon^{23}) \quad (4)$$

with T_b^{23} and T_b^{31} representing brightness temperatures at 23.8 and 31.4 GHz, respectively, T_s is the sea surface temperature, ω_v is the water vapour mass absorption coefficient, ω_l is cloud liquid water the mass absorption coefficient, τ_0 is the optical thickness, ε is the surface emissivity, and $\mu = cos\theta$, where θ is the satellite zenith angle.

Unfortunately, the measurements at 23.8 and 31.4 GHz are not available for MWTS onboard FY-3A. However, the observations from different channels are not uncorrelated. In this study, we find that the observations at frequencies of 50.3 and 53.6 GHz can be utilised to derive LWP index using following empirical equation:

$$L_{index} = c_0 + c_1 log(T_s - T_b^{50}) + c_2 log(T_s - T_b^{53}) \quad (5)$$

where $T_b^{50}$and $T_b^{53}$are the MWTS measurements at frequencies of 50.3 GHz and 53.6 GHz respectively, and T_s is the sea surface temperature. Before applying the observations from these channels, MWTS channel frequency-drift introduced bias has been firstly corrected (Wang et al. 2012). The scan angle dependent coefficients c_0, $c_1$and c_2 obtained using regression method based on 'training' samples are shown in Table 2. Similarly, this algorithm can be utilised to calculate LWP index for MetOp-A AMSU-A based on the two channel measurements at the same frequencies. Also the coefficients are presented in Table 3. We can see that the coefficient c_0 decreases as scan angle increases, while the coefficients $c_1$and c_2 increase as the scan angle increases for both MWTS and AMSU-A.

Scan angle	C_0	C_1	C_2
48.3°	-0.3786	-0.6287	0.8761
41.4°	0.3461	-0.9086	0.7990
34.5°	1.4717	-1.0896	0.7554
27.6°	2.4896	-1.2009	0.6768
20.7°	3.2261	-1.2682	0.5684
13.8°	3.7958	-1.3075	0.4899
6.9°	4.1008	-1.3279	0.4435
0°	4.2002	-1.3343	0.4283

Table 2 The scan angle dependent regression coefficients for FY-3A MWTS.

Scan angle	C_0	C_1	C_2
48°20′	-0.0191	-0.5830	0.7789
45°00′	0.1570	-0.7263	0.7772
41°40′	0.5111	-0.8518	0.7516
38°20′	0.9683	-0.9570	0.7301
35°00′	1.4630	-1.0429	0.7090
31°40′	1.9506	-1.1117	0.6601
28°20′	2.4045	-1.1663	0.6225
25°00′	2.8109	-1.2094	0.6110
21°40′	3.1638	-1.2430	0.5652
18°20′	3.4617	-1.2690	0.5246
15°00′	3.7056	-1.2887	0.4904
11°40′	3.8974	-1.3034	0.4629
8°20′	4.0390	-1.3137	0.4423
5°00′	4.1322	-1.3203	0.4286
1°40′	4.1785	-1.3235	0.4218

Table 3 Same as Table 2 except for MetOp-A AMSU-A.

3.2 Validation

In this study, MetOp-A AMSU-A cloud LWP index over ocean within 55°S–55°N during 1–5 January 2010 is firstly calculated using Eqn 2, meanwhile, the AMSU-A cloud LWP products based on Eqn 1 are obtained from the operational microwave surface and precipitation products system (MSPPS). In order to validate the effectiveness of the new cloud detection method, the scatter plots of AMSU-A cloud LWP index and LWP are displayed in Figure 1. For simplicity, logarithmic coordinates are used, and only results over FOVs 4, 7, 11 and 15 are given. The total numbers within each 0.2 kg/m^2 interval box indicated by colour are taken into consideration. The fitted quadratic lines show that great correlation between cloud LWP index and LWP, which can demonstrate that the new cloud detection algorithm is reasonable in some sense. Generally, a cloud LWP of 0.05 kg/m^2 is used as a threshold for detecting cloud-affected microwave radiance and 0.5 kg/m^2 used as the threshold for heavy precipitation (Weng et al. 2012). AMSU-A cloud LWP index variations as FOVs based on the quadratic regression at the LWP values of 0.05 kg/m^2 and 0.5 kg/m^2 are shown in Figure 2a. The LWP indexes are almost the same except for large scan angle corresponding to the threshold value of 0.05 kg/m^2, while they are much different among different scan angle corresponding to the heavy rain threshold. The LWP index used as heavy rain detection is much larger at nadir than swath edge. Then the AMSU-A LWP indexes threshold for cloud and heavy rain detection are interpolated into MWTS FOVs according to the scan angle (see Figure 2b). Hereafter, the MWTS LWP indexes threshold for cloud and heavy rain are denoted as L_1 and L_2 respectively.

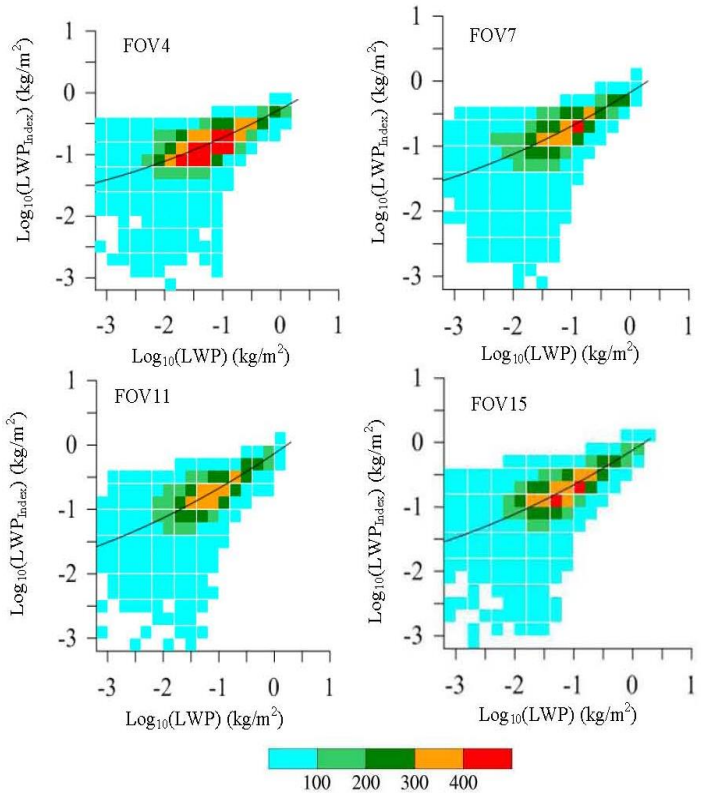

Figure 1 Total number within 0.2 kg/m2 interval of AMSU-A LWP index and LWP for FOVs 4, 7, 11 and 15 over ocean within 55°S–55°N using data during 1–5 January 2010. The quadratic lines are also presented in each panel.

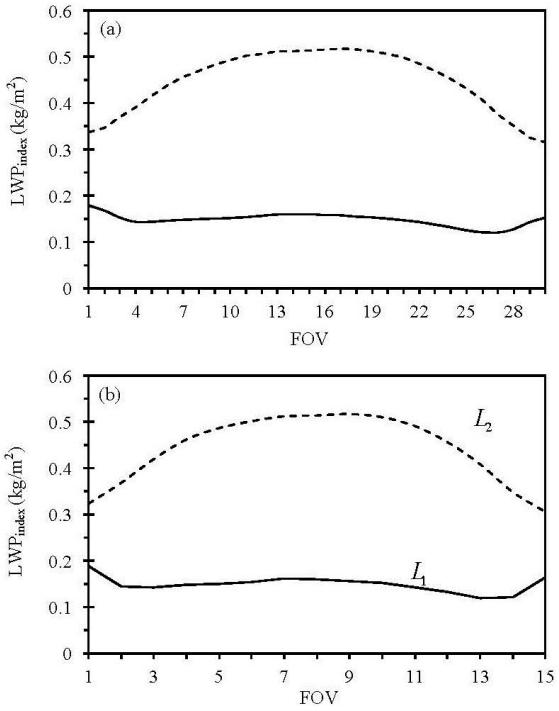

Figure 2 (a) LWP index variations as FOV based on the quadratic regression at the LWP value 0.05 kg/m^2 (solid line) and 0.5kg/m^2 (dashed line); (b) same as (a) except for interpolating into MWTS FOVs.

MWTS cloud LWP indexes over ocean during entire January 2010 are also calculated using Eqn 2. Figure 3 shows the scatter plots of brightness temperature differences between MWTS channels 1–2 observations and simulations and MWTS LWP indexes within 30°S-30°N and 90°W-180°W over ocean from 0300 UTC–1500 UTC on 1 January 2010. The grey dots indicate the data points with LWP index values being above the solid line L_1 shown in Figure 2b. The O-B difference of MWTS channel 1 is small under clear sky condition, however, the difference increases quickly as the LWP index increases, which demonstrates that the observations are contaminated by cloud. MWTS channel 1 is sensitive to surface, and the surface emissivity over ocean is about 0.5, much smaller than that of cloud. Moreover, the cloud emission effect of MWTS channel 1 dominates than scattering, while the scatting effect is much more important than emission for MWTS channel 2. So we can see the bias between observation and simulation difference increases sharply as LWP index increases. Figure 4 shows the distributions of MWTS and AMSU-A observed FOVs when the values of two variables LWP index (L_{index}) and LWP (L) are within three different ranges for data during 0300 UTC–1500 UTC on 1 January 2010. Note that the MWTS swaths do not overlap the AMSU-A swaths because of the different equator crossing time and the size of data points plotted in this figure does not reflect the increase of FOV size with scan angle. Also keep in mind that MWTS observation resolutions are coarser than AMSU-A observations. For example, MWTS FOV diameter at nadir is 62 km, while the diameter AMSU-A FOV a t nadir is about 48 km. However, the general patterns of cloudy FOVs are greatly comparable between Figures 4(a) and 4(b). Results using LWP index for cloud detection compare well with those of LWP over their overlapping portions of swaths. For quantitative analysis, the MWTS observed FOVs and AMSU-A FOVs are collocated under the criteria of spatial distance of 30 km and temporal difference of three hours using data during entire 2010, so that the cloudy MWTS FOVs can be detected by both LWP and LWP index. Figure 5 displays the global percentages of four kinds of combinations, saying, cloudy MWTS FOVs are identified by both LWP index and LWP, only identified by LWP index, as well as clear-sky FOVs are identified by both LWP index and LWP, and only identified by LWP index for all data over ocean in January 2010. The percentages of the four cases are 46.9%, 14.7%, 26.6% and 11.8% respectively. The total percentage of the consistent results from these two cloud detection methods is about 73.5%, which demonstrates the LWP index algorithm performs well.

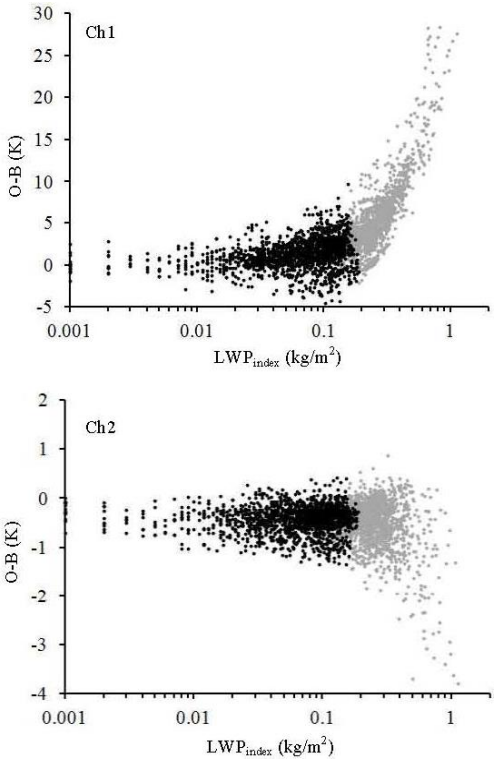

Figure 3 The scatter plots of brightness temperature differences between MWTS channels 1–2 observations and simulations and MWTS LWP index within 30°S–30°N and 90°W–180°W over ocean from 0300 UTC–1500 UTC on 1 January 2010. The data whose LWP index is above the L1 in Figure 2b is indicated by grey dots.

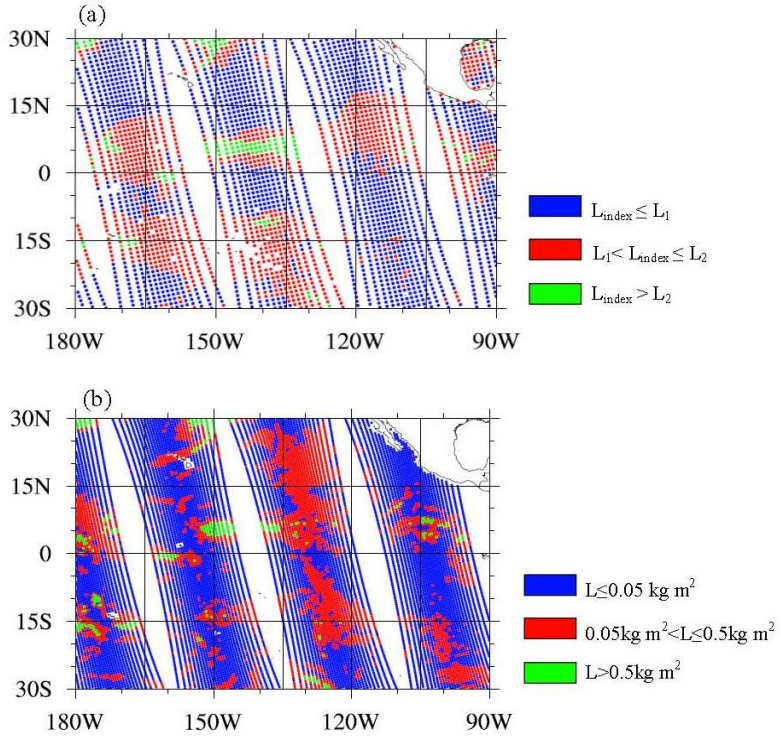

Figure 4 Distributions of observed FOVs when values of two variables (a) LWP index, (b) LWP are three different ranges for data during 0300 UTC–1500 UTC 1 January 2010.

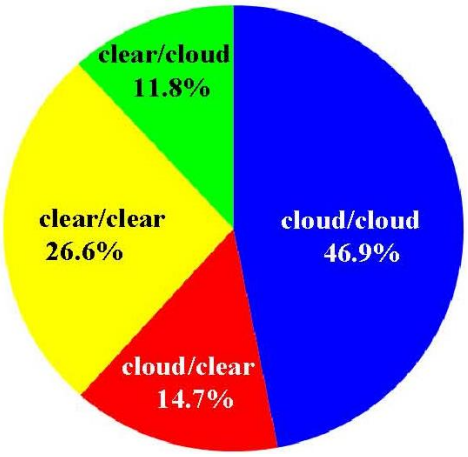

Figure 5 Global percentages of cloudy MWTS FOVs identified by both LWP index ≥ L1 and LWP ≥ 0.05 kg/m^2 (blue) or only by LWP index ≥ L1 (red), as well as global percentages of clear-sky FOVs identified by both LWP index < L1 and LWP < 0.05 kg/m2 (yellow) or only by LWP index < L1 (green) for all data over ocean in January 2010.

4. QC procedures and results

MWTS radiances can provide useful atmospheric temperature information in non-precipitating cloudy conditions. However, cloudy radiances are removed in most assimilation system due to insufficient cloud fields output from NWP models required by radiative transfer model, a non-constant bias in the presence of clouds, and the reduced accuracy of radiative transfer model for simulating cloudy radiances. In addition, surface emissivity that varies with frequency, surface type, soil content, surface wind, vegetation and viewing angle brings another type of challenge for satellite data assimilation. The large uncertainty in surface emissivity makes the simulations of surface-sensitive channels in less agreement with observations, especially over land, snow, sea ice, and coastal areas. Besides, abnormal observations may happen due to instrument problems or human mistakes. The purpose of quality control procedures are not only removing the cloud contaminated and surface effected radiances, but also those data that could not be well simulated. In this study, the quality control used for the elimination of MWTS observations is executed sequentially in the following order: (1) coastal observations of channels 2 and 3 are removed; (2) observations of channel 2 over sea ice, or land are removed; (3) cloudy observations of channel 2 and 3 with LWP index above L1 are identified and removed; and (4) the remaining outliers identified by the biweighting (Zou and Zeng 2006) check are eliminated.

Figure 6 shows scatter plots of the differences of brightness temperature between MWTS channels 2–4 observations and model simulations on 1 January 2011. Outliers removed by specific quality control procedure are indicated in colours. The observations minus simulations differences of outliers and their standard deviations are much larger than those of the remaining data after quality control. For channel 2, the observed brightness temperature could be more than 10 K colder or warmer than model simulations due to surface emissivity uncertainty and cloud effect. The data spread for all three channels is significantly reduced after quality control, and the temperature dependency can not be seen obviously from observations minus simulations differences. Figure 7 shows the global distributions of observations minus simulations differences during 0300 UTC-1500 UTC at channels 2–4 for data that pass quality control. All the data differences are within ±2 K.

The 5-degree interval latitudinal angular biases of the MWTS channels 2–4 for the entire month of January 2010 are presented in Figure 8. It is noted that the size of the FOV increases with increasing scan angle. The larger the FOV is, the higher the atmospheric inhomogeneity is within the FOV. It is not only difficult to accurately simulate the atmospheric inhomogeneity within FOVs at larger scan angles in radiative transfer models, but also difficult to take the atmospheric inhomogeneity into account in the forward model and calibration process. These biases should be subtracted from observations minus simulations differences in the formulation of data assimilation. It can be seen that large negative scan biases

are presented at large scan angles at all latitudes for channels 2 and 3 at both sides of the scan lines before quality control. Relatively large negative scan biases for channel 4 are seen at large scan angles. The scan biases become small and not strong latitudinal dependence after quality control.

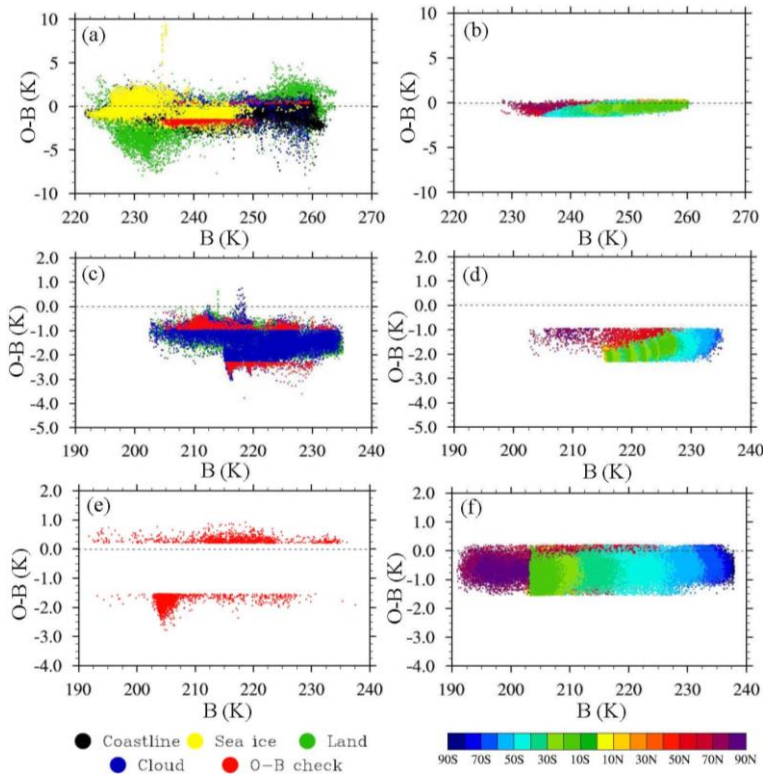

Figure 6 Scatter plots of the differences of brightness temperature between observations and model simulations for MWTS (a–b) channel 2, (c–d) channel 3 and (e–f) channel 4 outliers (left panels) and data that pass quality control (right panels) on 1 January 2010.

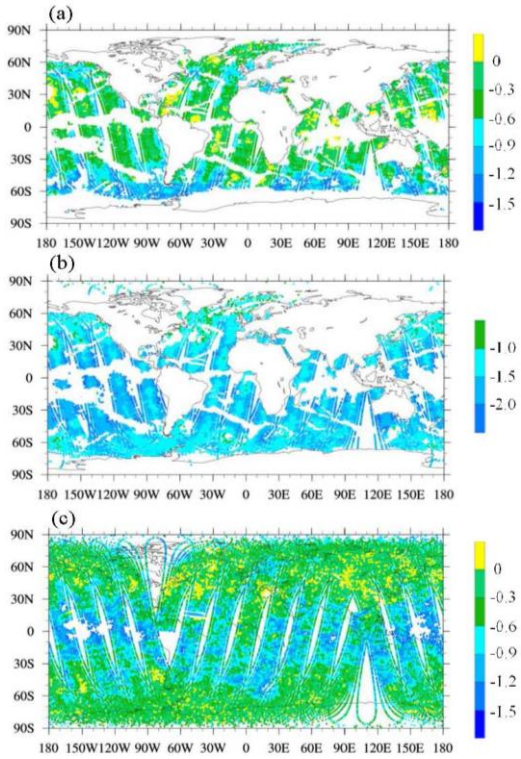

Figure 7 Global distribution of brightness temperature differences between MWTS observations and model simulations for the remaining data after (right panels) quality control during 0300 UTC–1500 UTC 1 January 2010. (a): channel 2, (b) channel 3 and (c) channel 4.

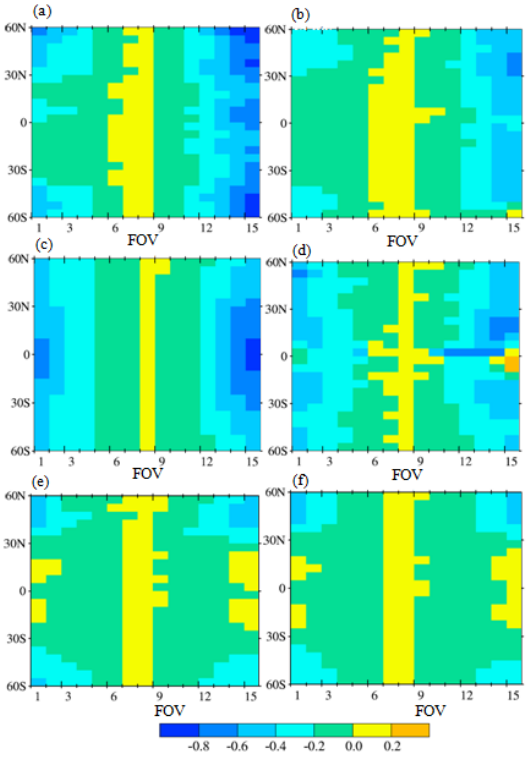

Figure 8 Latitudinal dependences of scan biases before (left panels) and after (right panels) quality control. Nadir biases are subtracted. (a–b) channel 2, (c–d) channel 3 and (e–f) channel 4.

Figure 9 presents the frequency distributions of observations minus simulations differences before and after quality control for MWTS channels 2–4. There is one thing to note that the angular biases are removed for the frequency distributions of data after quality control. We can obvious see that the frequency distributions of all data are asymmetric before quality control, and more data are located on the left-hand-side of the distributions. However, after quality control and bias correction, the bias and standard deviations of the brightness temperature differences between observations and model simulations are greatly reduced. Moreover, the frequency distributions become more Gaussian-like after quality control.

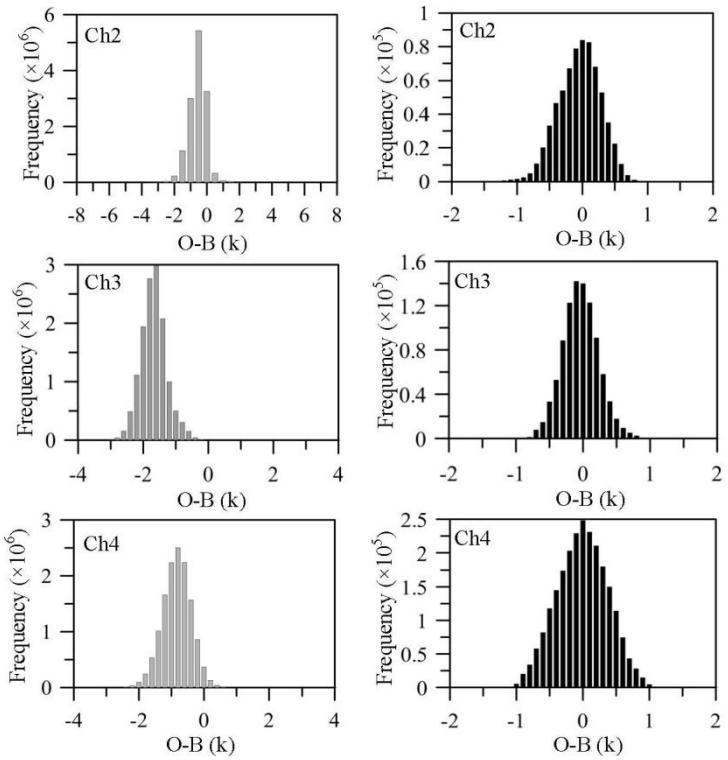

Figure 9 Frequency distributions of observations minus simulations differences for MWTS channels 2–4 before (left panels) and after (right panels) quality control. Biases are removed for the frequency distributions of data after quality control.

5. Summary and conclusions

The second generation of Chinese FY-3 polar-orbiting satellites, FY-3A/B/C, were successfully launched on 27 May 2008, 5 November 2010 and 23 September 2013, respectively. The experimental satellites FY-3A/B carried eleven sensors, while four more instruments were carried on the operational satellite FY-3C. MWTS is one of the important instruments onboard all the three satellites.

A new cloud detection scheme for MWTS is proposed based on the two channels' measurements at frequencies of 50.3 GHz and 53.6 GHz, and the accuracy of cloud detected results is further tested using MetOp-A AMSU-A cloud LWP products. Analysis indicates that the percentages of clouds from this new cloud detection algorithm are compared very well with those obtained from cloud LWP products. In general, the global percentages of cloud retrieved from the new algorithm are about two thirds. Besides cloud detection, measurements over land and sea ice are also eliminated for channels 2 or 3. Finally, outliers that deviate greatly from model simulated MWTS radiances are also removed. After quality control, FY-3A MWTS data show a more coherent pattern when compared to model simulations. The frequency distributions of the differences between observations and model simulations for all three MWTS sounding channels are more Gaussian-like after quality controls and bias corrections.

This work can be extended to the following FY-3 microwave temperature sounder measurements. The methodology will be incorporated into global/regional assimilation and prediction system (GRAPES) developed by China or other NWP modelling systems. Incorporating FY-3 vertical atmospheric sounding radiance data can increase the current global coverage of satellite observations in operational numerical weather prediction.

Acknowledgments

This work was jointly supported by Key Laboratory of South China Sea Meteorological Disaster Prevention and Mitigation of Hainan Province Grant No. SCSF201402 and The Startup Foundation for Introducing Talent of NUSIT S8113066001. Sincere thanks are given to National Satellite Meteorological Centre, Chinese Meteorology Administration for providing FY-3A MWTS data.

References

Andersson, E., Pailleux, J., Thepaut, J.N., Eyre, J.R., McNally, A.P., Kelly G.A. and Courtier. P. 1994, Use of cloud-cleared radiances in three-four-dimensional variational data assimilation, *Quart. J. Roy. Meteor. Soc*., 120, 627–653.

Baker, N. L. and Daley, R. 2000. Observation and background adjoint sensitivity in the adaptive observation-targeting problem. *Quarterly Journal of the Royal Meteorological Society*, 126(565), 1431-1454.

Bauer, P., Lopez, P., Benedetti, A., Salmond, D. and Moreau, E. 2006. Implementation of 1D+4D-Var assimilation of precipitation-affected microwave radiances at ECMWF. I: 1D-Var. *Quart. J. Roy. Meteor. Soc.*, 132, 2277–2306.

Bauer, P., Geer, A. J., Lopez, P. and Salmond, D. 2010. Direct 4D-Var assimilation of all-sky radiances. Part I: Implementation. *Quart. J. Roy. Meteor. Soc.*, 136, 1868–1807.

Cardinali, C. 2009. Monitoring observation impact on short-range forecast. *Quarterly Journal of the Royal Meteorological Society*, 135(638), 239–250.

Coutier, P., Andersson, E., Heckley, W., Pailleux, J., Vasiljevic, D., Hamrud, M., Hollingsworth, A., Rabier, F., Fisher, M. and Pailleux, J. 1998. The ECMWF implementation of three-dimensional variational assimilation (3D-Var). I: Formulation. *Quart. J. Roy. Meteor. Soc.*, 124, 1783–1807.

Derber, J.C. and Wu, W.S. 1998. The use of TOVS cloud-cleared radiances in the NCEP SSI analysis system. *Mon. Wea. Rev.*, 126, 2287–2299.

Dong, C., Yang, J., Zhang, W., Yang, Z., Lu, N., Shi, J., Zhang, P., Liu, Y. and Cai B. 2009. An overview of a new Chinese weather satellite FY-3A. *Bulletin of the American Meteorological Society*, 90(10), 1531–1544.

Fourrie, N., Doerenbecher, A., Bergot, T. and Joly, A. 2002. Adjoint sensitivity of the forecast to TOVS observations. *Quarterly Journal of the Royal Meteorological Society*, 128(586), 2759–2777.

Han, Y., Weng, F., Liu, Q. and Delst, P.V. 2007. A fast radiative transfer model for SSMIS upper atmosphere sounding channel. *J. Geophys. Res.*, 112, DOI:10.1029/ 2006JD008208.

Klaes, D. and Schraidt, R. 1999. The European ATOVS and AVHRR processing package (AAPP). *Tech. Proc.10th Int. ATOVS Study Conf., Boulder, 1999.*

Okamoto, K., Kazumori, M. and Owada, H. 2005. The assimilation of ATOVS radiances in the JMA global analysis system. *J. Meteor. Soc. Japan*, 83, 201–217.

Langland, R. H. and Baker, A.L. 2004. Estimation of observation impact using the NRL atmospheric variational data assimilation adjoint system. *Tellus series A- Dynamic Meteorology and Oceanography*, 56(3), 189–201.

Li J. and Zou, X. 2013. A quality control procedure for FY-3A MWTS measurements with emphasis on cloud detection using VIRR cloud fraction. *J. Atmos. Ocean Tech.*, 30, 1704–1715.

Li, J. and Zou, X. 2014. Impact of FY-3A MWTS radiances on prediction in GRAPES with comparison of two quality control schemes. *Frontiers of Earth Science*, 8(2), 251-263. DOI: 10.1007/s11707-014-0405-3.

McNally, A. P., Derber, J. C. and Wu, W. and Katz, B. 2000, The use of TOVS level-1b radiances in the NCEP SSI analysis system. *Quart. J. Roy. Meteor. Soc.*, 126, 689–724.

Mo, T. 1999. Calibration of the advanced microwave sounding unit-A radiometers for NOAA-L and NOAA-M. NOAA Technical Report NESDIS 92, 53 pp.

Wang, X., Zou, X., Weng, F. and You, R. 2012. An assessment of the FY-3A Microwave Temperature Sounder using the NCEP numerical weather prediction Model. *IEEE Trans. Geosci. Remote Sens.*, 50(12), 4860–4874.

Weng, F. and Grody, N.C. 1994. Retrieval of cloud liquid water over oceans using special sensor microwave imager (SSM/I). *J. Geophys. Res.*, 99, 25535–25551.

Weng, F., Zhao, L., Ferraro, R., Poe, G., Li, X. and Grody, N. 2003. Advanced Microwave Sounding Unit Cloud and Precipitation Algorithms. *Radio Sci.*, 38, 8086–8096.

Weng, F. 2007. Advances in radiative transfer modelling in support of satellite data assimilation. *J. Atmos. Sci.*, 64, 3799–3807.

Weng, F., Zou, X., Wang, X., Yang, S. and Goldberg, M. D. 2012. Introduction to Suomi NPP ATMS for NWP and tropical cyclone applications. *J. Geophy. Res.*, 117, D19112, 14 pp., doi:10.1029/2012JD018144.

Yang, J., Dong, C., Lu, N., Yang, Z., Shi, J., Zhang, P., Liu, Y. and Cai, B. 2009. Chinese new generation of polar-orbiting satellites FY-3. *Acta Meteorologica Sinica*, 67, 501–509.

You, R., Gu, S., Guo, Y., Chen, W. and Yang, H. 2012. Long-term calibration and accuracy assessment of the FengYun-3 Microwave Temperature Sounder Radiance Measurements. *IEEE Trans. Geo. Remote Sensing*, 50(12), 4854–4859.

Zhang, H., Xue, J., Zhu, G., Zhuang, S., Wu, X. and Zhang, F. 2004. Application of direct assimilation of ATOVS microwave radiances to typhoon track prediction. *Adv. Atmos. Sci.*, 21(2), 283–290.

Zou, X. and Zeng, Z. 2006. A quality control procedure for GPS radio occultation data. *J. Geoph. Res.*, 111, D02112, doi:10.1029/2005JD005846.